Enantioselective Surface Chemistry of *R*-2-bromobutane on Cu(643)$^{R\&S}$ and Cu(531)$^{R\&S}$

D. M. Rampulla,[†] A. J. Francis,[‡] K. S. Knight,[§] and A. J. Gellman*[,†]

Department of Chemical Engineering and Department of Materials Science and Engineering, Carnegie Mellon University, Pittsburgh, Pennsylvania 15213, and Department of Chemistry, University of Tennessee—Chattanooga, Chattanooga, Tennessee 37403

Received: January 24, 2006; In Final Form: March 26, 2006

The enantioselective surface chemistry of chiral *R*-2-bromobutane was studied on the naturally chiral Cu(643)$^{R\&S}$ and Cu(531)$^{R\&S}$ surfaces by comparing relative product yields during temperature-programmed reaction spectroscopy. Molecularly adsorbed *R*-2-bromobutane can desorb molecularly or debrominate to form *R*-2-butyl groups on the surfaces. The *R*-2-butyl groups react further by β-hydride elimination to form 1- or 2-butene or by hydrogenation to form butane. Temperature-programmed reaction spectroscopy was used to quantify the relative yields of the various reaction products. At low coverages of *R*-2-bromobutane on Cu(643)$^{R\&S}$ and Cu(531)$^{R\&S}$, the surface chemistry is not enantioselective. At monolayer coverage, however, the product yields indicate that the *R*-2-bromobutane decomposition reaction rates are sensitive to the handedness of the two chiral surfaces. The impact of surface structure on enantioselectivity was examined by studying the chemistry of *R*-2-bromobutane on both Cu(643)$^{R\&S}$ and Cu(531)$^{R\&S}$. The selectivity of *R*-2-bromobutane desorption versus debromination is enantiospecific and differs significantly from Cu(643) to Cu(531). The selectivity of the *R*-2-butyl reaction by β-hydride elimination versus hydrogenation is only weakly enantiospecific and is similar on both the Cu(643) and Cu(531) surfaces. These results represent the first quantitative observations of enantioselectivity in reactions with well-known mechanisms probed using a simple adsorbate on naturally chiral metal surfaces.

1. Introduction

If an object and its mirror image are nonsuperimposable, they are chiral. Chirality is a critical property of the amino acids that form proteins, the building blocks of life on Earth. Chirality is often expressed in complex biological molecules, pharmaceuticals, and agrochemicals in the form of carbon atoms that are tetrahedrally coordinated to four different organic groups. Practically, the importance of molecular chirality arises from the fact that the two mirror images of a chiral molecule, known as enantiomers, can have vastly different physiological impacts when ingested by living organisms. As a result, chiral compounds such as pharmaceuticals that are produced for human consumption must be produced in enantiomerically pure form. Understanding enantioselectivity is critical to the development of methods for the detection, separation, and reaction of chiral compounds. Such enantioselective processes require a chiral medium, such as a surface, to discriminate between the two enantiomers of a chiral compound.

Most chiral surfaces are prepared by irreversibly adsorbing chiral ligands to an achiral surface, and it is the chiral ligand that imparts chirality.[1,2] A second type of chiral surface can be created by cleaving a crystalline material that possesses a bulk chiral structure by virtue of having a chiral unit cell.[3,4] A third type of "naturally chiral" surface can be prepared by exposing a high Miller index plane of an achiral crystalline material such as a metal. Naturally chiral metal surfaces can be more reactive than surfaces of bulk chiral materials, which tend to be inorganic oxides, and are certainly more thermally stable than organic chiral surfaces. Thus naturally chiral metal surfaces are attractive candidates for enantioselective processes.

Naturally chiral surfaces of face-centered cubic (fcc) metals have structures formed of terraces separated by monatomic height steps and kinks. The kinks are chiral adsorption sites at which enantioselective surface chemistry can occur. These kinks are formed by the intersection of three microfacets of the three low Miller index planes: (111), (100), and (110). A sense of rotation exists among these microfacets and can be used to assign their chirality by prioritizing them in order of decreasing atomic packing density [(111) > (100) > (110)].[5−7] Figure 1 shows the ideal atomic structure of the Cu(643)^{R} and Cu(531)^{S} surfaces used in these experiments. Cu(643) surfaces have structures formed by kinked step edges that are separated by (111) terraces that are approximately three atoms wide. Along the step edge, each kink is separated by two unit cell lengths of the (100) microfacet. Cu(531) is a unique chiral surface because it is formed by the intersections of single unit cells of the (111), (100), and (110) microfacets. As a consequence, it has the highest possible density of chiral kinks. The Cu(643) and Cu(531) surfaces were chosen in order to study the impact of different surface structures on the enantioselectivities of reactions involving chiral adsorbates.

Research performed over the past few years has led to an increased understanding of the enantioselective properties of naturally chiral metal surfaces. Gellman et al. first postulated that the naturally chiral, high Miller index planes of fcc metals ought to exhibit enantiospecific surface chemistry.[8] Atomistic simulations of the interactions of small chiral hydrocarbons with chiral platinum surfaces performed by Sholl showed that such

* Corresponding author. E-mail: gellman@cmu.edu. Telephone: 412-268-3848.
[†] Department of Chemical Engineering, Carnegie Mellon University.
[‡] Department of Materials Science and Engineering, Carnegie Mellon University.
[§] Department of Chemistry, University of Tennessee—Chattanooga.

10.1021/jp060508+ CCC: $33.50
Published on Web 05/09/2006

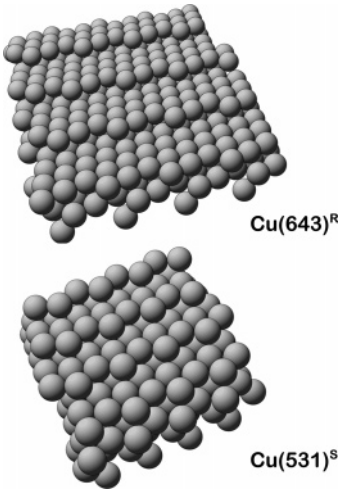

Figure 1. Ideal structures of the chiral Cu(643) and Cu(531) surfaces.

enantioselectivity should occur and that it should be possible to observe enantiospecific differences between adsorption energies of the enantiomers of chiral molecules on naturally chiral surfaces.[9] Recently, temperature-programmed desorption studies of *R*- and *S*-propylene oxide[10,11] and *R*-3-methylcyclohexanone[10,12] on the Cu(643)^R and Cu(643)^S surfaces have revealed enantiospecific desorption energies.

Attard et al. have explored the electrooxidation of chiral sugars in aqueous solutions on chiral and achiral Pt electrodes.[5,13,14] Their results revealed that the electrooxidation rates are enantioselective on a number of chiral platinum surfaces, but the reaction mechanism is complicated and it is not clear which of the elementary steps in the overall reaction mechanism give rise to enantioselectivity. Furthermore, the large number of chiral centers on these sugars obfuscates the underlying interaction between the chiral molecule and the chiral surface.

The chiral copper surfaces chosen to study the impact of surface structure on enantioselectivity were Cu(643)$^{R\&S}$ and Cu(531)$^{R\&S}$. In this work, *R*-2-bromobutane, $CH_3{}^*CH(Br)CH_2CH_3$, was used as the chiral reactant because it has a predictable reaction mechanism with known intermediates and products, as illustrated in Figure 2.

$$CH_3{}^*CH(Br)CH_2CH_{3(a)} \xrightarrow{k_1} CH_3{}^*CH(Br)CH_2CH_{3(g)}$$
desorption of *R*-2-bromobutane (1)

$$CH_3{}^*CH(Br)CH_2CH_{3(a)} \xrightarrow{k_2} Br_{(a)} + CH_3{}^*\dot{C}HCH_2CH_{3(a)}$$
debromination of *R*-2-bromobutane (2)

$$CH_3{}^*\dot{C}HCH_2CH_{3(a)} \xrightarrow{k_3} CH_3CH{=}CHCH_{3(a)} + H_{(a)}$$
β-hydride elimination of *R*-2-butyl (3)

$$CH_3{}^*\dot{C}HCH_2CH_{3(a)} + H_{(a)} \xrightarrow{k_4} CH_3CH_2CH_2CH_{3(a)}$$
hydrogenation of *R*-2-butyl (4)

$$CH_3CH{=}CHCH_{3(a)} \xrightarrow{k_5} CH_3CH{=}CHCH_{3(g)}$$
desorption of butene (5)

$$CH_3CH_2CH_2CH_{3(a)} \xrightarrow{k_6} CH_3CH_2CH_2CH_{3(g)}$$
desorption of butane (6)

There are two competing reaction pathways for reaction of alkyl bromides adsorbed on Cu surfaces: molecular desorption or debromination to produce adsorbed alkyl groups.[15,16] The adsorbed alkyl groups then react via two competing pathways: β-hydride elimination to produce olefins or hydrogenation to produce alkanes.[16−20] Thus the reaction of an alkyl halide yields three desorbing products: the alkyl halide, olefins, and alkanes.

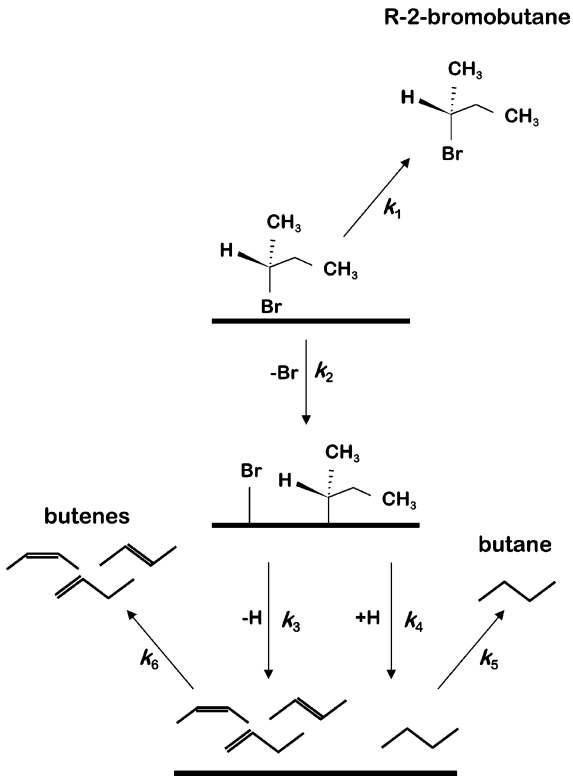

Figure 2. Reaction mechanism of *R*-2-bromobutane on Cu surfaces. Adsorbed *R*-2-bromobutane can either desorb molecularly or debrominate to produce an *R*-2-butyl intermediate. *R*-2-butyl undergoes β-hydride elimination to produce butenes or hydrogenation to produce butane. Butenes and butane then desorb molecularly.

Product yields were used to quantify the enantioselectivities of reactions 1−4, each of which can have an enantiospecific reaction rate constant on a chiral surface. The enantioselectivities of the four reactions are defined as follows and are based on the product yields.

Desorption: $$ES_{des} = \frac{Y^{R/R}_{bromobutane}}{Y^{R/S}_{bromobutane}}$$

Debromination: $$ES_{Br} = \frac{Y^{R/R}_{2-butyl}}{Y^{R/S}_{2-butyl}} = \frac{Y^{R/R}_{butene} + Y^{R/R}_{butane}}{Y^{R/S}_{butene} + Y^{R/S}_{butane}}$$

β-Hydride elimination: $$ES_{\beta H} = \frac{Y^{R/R}_{butene}}{Y^{R/S}_{butene}}$$

Hydrogenation: $$ES_{H} = \frac{Y^{R/R}_{butane}}{Y^{R/S}_{butane}}$$

Here, $Y^{R/R}_{butane}$ refers to the yield of butane generated during temperature-programmed reaction of *R*-2-bromobutane on the Cu(*hkl*)^R surface. Note that a value of $ES = 1$ indicates a process that is not enantioselective. The details of the analysis of the measured signals to determine the enantioselectivities are given in Appendix A.

The primary result of the work presented in this paper is the observation that the surface chemistry of *R*-2-bromobutane on

the Cu(643)$^{R\&S}$ and Cu(531)$^{R\&S}$ surfaces is enantioselective and, moreover, that the enantioselectivity is dependent on the surface structure. The work also demonstrates that, under conditions in which reactions are 100% selective to a given product, one cannot observe enantioselectivity, although the underlying reaction rate constants may be enantiospecific. A secondary result of the work is the demonstration of the use of X-ray diffraction to determine the absolute orientations of the Cu(531)$^{R\&S}$ surfaces, which cannot be determined from low-energy electron diffraction patterns.

2. Experimental Section

2.1. Equipment and Procedure. The surface analysis and surface chemistry measurements were made in an ultrahigh vacuum (UHV) chamber evacuated by an ion pump. The UHV chamber is equipped with an Ar^+ gun for cleaning the copper surfaces. Low-energy electron diffraction (LEED) optics were used to determine the order of the Cu crystal surfaces after cleaning and to determine the absolute orientation of the Cu(643)$^{R\&S}$ surfaces. The chamber also contained an Extrel quadrupole mass spectrometer shrouded in a stainless steel housing with a 9 mm aperture to the ionizer. The mass spectrometer was used to identify vapors introduced into the UHV chamber and for temperature-programmed reaction spectroscopy (TPRS) measurements.

The Cu(643) and Cu(531) samples were obtained from Monocrystals Co. The Cu(643) sample was a single-crystal disk that is 12.5 mm in diameter and 2 mm thick, which exposed the (643)^S surface on one side and the (643)^R surface on the other. The Cu(531) sample was a single-crystal disk that was 10 mm in diameter and 2 mm thick and exposed both the (531)^S and (531)^R surfaces. The absolute orientation or handedness of the Cu(643) surfaces were determined from their LEED patterns; however, determination of the orientations of the Cu(531) surfaces required the use of X-ray diffraction (XRD). XRD was performed using a three-circle Philips X'Pert X-ray diffractometer prior to putting the Cu(531) sample into the UHV chamber.

In the UHV chamber, the crystals were individually mounted on a manipulator allowing *xyz* motion and rotation about the vertical axis of the chamber. The samples were spot-welded between two Ta wires and could be heated resistively to $T > 1000$ K. The samples could also be cooled to $T < 100$ K through mechanical contact with a liquid nitrogen reservoir. The temperature of the samples was measured using a K-type thermocouple that was spot-welded to the perimeter of the sample disk.

Once mounted in the chamber, the surfaces were cleaned by cycles of Ar^+ bombardment to remove surface contaminants. During cleaning, the ion current measured on the sample was 5 μA at an ion energy of 2.5 keV. After ion bombardment, the copper samples were annealed at 1000 K for 10 min. A sharp LEED pattern verified the surface order of the crystals.

Racemic 2-bromobutane was purchased from Acros with a purity of >99%. *R*-2-Bromobutane was synthesized by brominating *S*-2-butanol with phosphorus tribromide.[21] A 100 mL Schlenk flask was attached to a nitrogen manifold and equipped with a septum and a magnetic stir bar. The flask was charged with 1.0 g of *S*-2-butanol (99%, Aldrich Chemical Co.) and cooled to $-5°$ C in a bath containing ice and saturated NaCl solution. A 1.4 mL portion of PBr_3 was added to the flask dropwise through a syringe over the course of 2 h. The reaction mixture was then allowed to warm to room temperature and was stirred for 12 h. The reaction mixture was then cooled in an ice bath and quenched by the addition of 10 mL of water and then extracted into 10 mL of diethyl ether. The ether solution was dried over sodium sulfate, concentrated, and distilled, yielding 2.08 g of product (61% chemical yield). The enantiomeric excess was determined to be 97% by using chiral gas chromatography on an Agilent 6850 GC, equipped with a Supelco Betadex 225 column.

Racemic 2-bromobutane and *R*-2-bromobutane were transferred to individual glass vials, which were attached to stainless steel vacuum lines connected to the UHV chamber via a leak valve. Before introduction into the chamber, each compound was subjected to cycles of freezing, pumping, and thawing to remove air and other high vapor pressure contaminants. Mass spectroscopy was used to verify the purity of each sample. During exposure of the surfaces to vapor, the pressure was measured using the ion gauge. Exposures for each compound are reported in Langmuirs ($1\ L = 10^{-6}$ Torr·s) and are not corrected for ion gauge sensitivity factors.

After cleaning the Cu surfaces, the desired adsorbate coverages were obtained by holding the sample temperature at 150 K and exposing it to either 1 L (2×10^{-8} Torr, 50 s) or 7 L (1.4×10^{-7} Torr, 50 s) of either *R*- or *rac*-2-bromobutane vapor. The monolayer coverage was achieved by exposing the sample at 150 K to 7 L of vapor. The sample was held at 150 K during exposure to avoid multilayer formation. Higher exposures at lower temperatures resulted in the adsorption of multilayer films.

After adsorption of the desired coverages of *R*- or *rac*-2-bromobutane on the surfaces at 150 K, TPRS experiments were performed. The Cu sample was cooled to below 100 K and then moved to a position approximately 3−4 mm from the aperture of the mass spectrometer. The sample was then heated at a constant rate of 1 K/s, while using the mass spectrometer to monitor signals at $m/q = 56$, 57, and 58. These m/q ratios are characteristic of the fragmentation patterns of the species desorbing from the surface: 2-bromobutane, butane, and butene. After each TPRS experiment, the surface was cleaned by Ar^+ bombardment to remove bromine.

TPRS of *rac*-2-bromobutane was used as a control experiment to verify that differences in the TPRS spectra of *R*-2-bromobutane on the two enantiomeric surfaces of a given sample are indeed due to enantiospecific effects. Because racemic 2-bromobutane is achiral, its TPR spectra are insensitive to the chirality of the surface; thus, any differences in TPR spectra obtained from *R*-2-bromobutane adsorbed on the two surfaces of a given sample can be attributed to enantiospecific effects.

The raw TPR spectra obtained by monitoring signals at $m/q = 56$, 57, and 58 were used to obtain the TPR spectra of the three surface reaction products (2-bromobutane, butane, and butene). The fragmentation patterns of 2-bromobutane, butane, 1-butene, *cis*-2-butene, and *trans*-2-butene were measured over a range of pressures using the mass spectrometer. The fragmentation patterns of 1-butene, *cis*-2-butene, and *trans*-2-butene are almost identical. Thus they cannot be distinguished using the mass spectrometer and we are only able to report the total yield of butenes from the mass spectrometry data. Using the fragmentations patterns, the raw TPR spectra collected at $m/q = 56$, 57, and 58 were linearly decomposed to yield the TPR spectra of the 2-bromobutane, butane, and butene (Appendix A).

3. Results

3.1. Determination of the Chirality of the Cu(643) and Cu(531) Surfaces. LEED can be used to determine the chirality of the enantiomorphic faces of most chiral metal surfaces because the diffraction patterns from each face are chiral,

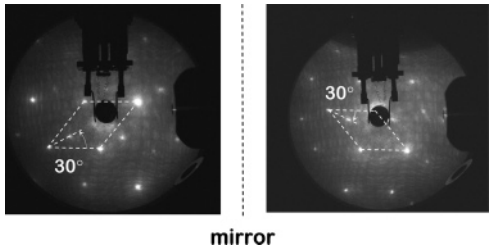

Figure 3. LEED patterns of Cu(531)$^{R\&S}$. The patterns are superimposable mirror images because the surface unit cell is rhombohedral.

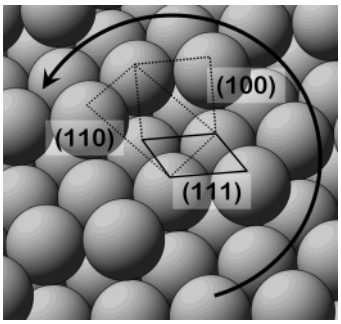

Figure 4. Microfacet structure of the Cu(531) surface. Although the shape of the surface unit cell is achiral, the sense of rotation among the three microfacets within the unit cell renders the structure chiral.

nonsuperimposable mirror images of one another. This arises simply from the fact that the unit cells of most stepped and kinked high Miller index surfaces are oblique and thus chiral. The chirality of each face of the Cu(643) sample (Figure 1) was determined using LEED.[22]

The determination of the chirality of the faces of Cu(531) (Figure 1) was less trivial. The unit cell of the Cu(531) surface lattice is rhombohedral and, thus, achiral. As a consequence, the LEED patterns of the (531) and ($\bar{5}\bar{3}\bar{1}$) surfaces are superimposable mirror images of one another, as seen in Figure 3. Although the unit cell of the surface lattice is achiral, the orientations of the microfacets that form the basis of the surface unit cell are nonsuperimposable and render these surfaces chiral. Figure 4 shows the microfacet structure of the (531)^{S} surface. The sense of rotation among the (111), (110), and (100) microfacets dictates the chirality of the surface. Unfortunately, this chirality is not reflected in the positions of the spots in the LEED pattern, and alternate means must be used to determine the chirality of the (531) surfaces.

XRD was used to determine the chirality of the (531) and ($\bar{5}\bar{3}\bar{1}$) faces of the Cu(531) crystal. It should be stated that {531} peaks cannot be observed directly by X-ray diffraction. The Bragg diffraction condition, $\lambda = 2d\cdot\sin\theta$, requires an interplanar d-spacing large enough that $2\theta < 180°$, which is not the case for any {531} planes given the X-ray wavelength used in this particular diffractometer. Even if this restriction were not present, XRD would be insufficient to index the two surfaces because diffracted intensity from any (hkl) and ($\bar{h}\bar{k}\bar{l}$) planes would occur at the same angles.

To observe diffracted intensity from the crystal, Bragg peaks were located by rotating the crystal through polar and azimuthal angles with respect to the normals of the (531) and ($\bar{5}\bar{3}\bar{1}$) planes. In this experiment, the (111), (200), (220), and (331) peaks were selected for the (531) surface (and their respective opposites for the ($\bar{5}\bar{3}\bar{1}$) face). The sample was rotated on the goniometer by a polar angle, ψ, that corresponds to the polar angle between the surface normal and the normal to the (hkl) plane being investigated. The 2θ value was then fixed to the value calculated for the (hkl) planes from Bragg's law, and a ϕ-scan (azimuthal

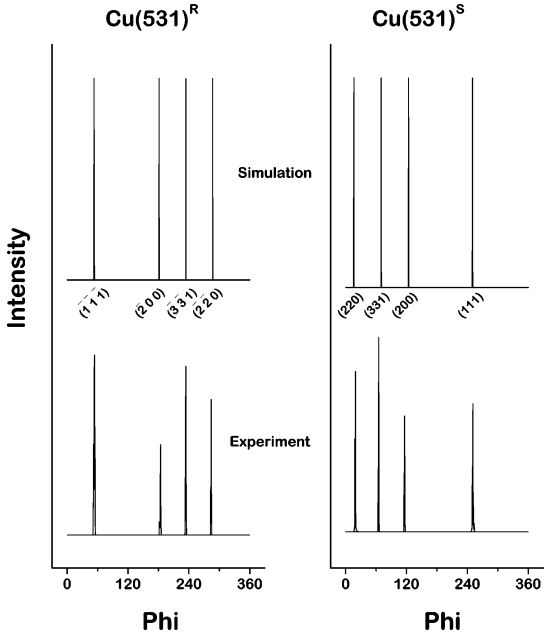

Figure 5. Comparison of simulated and experimental XRD spectra for Cu(531)$^{R\&S}$. XRD can be used to determine the absolute orientation of a chiral surface by observing the order of appearance of selected diffraction planes.

scan) was conducted to locate the diffraction peak. Because {531} surfaces lack rotational symmetry, only one peak will be observed in each of these ϕ-scans.

On the basis of a single Bragg peak from each surface, the (531) and ($\bar{5}\bar{3}\bar{1}$) surfaces cannot be distinguished from one another. However, by recording several ϕ-scans at the polar angles of several different planes, it is possible to distinguish the two sides of the crystal on the basis of the difference between the azimuthal angles of any two Bragg peaks obtained from one side of the crystal. Construction of a composite diffractogram, shown in Figure 5, using four ϕ-scans (obtained at the polar angles, ψ, associated with the (111), (200), (220), and (331) planes) reveals differences between the (531) and($\bar{5}\bar{3}\bar{1}$) surfaces. The patterns of the spacings between the peaks are clearly inverted between the two surfaces. Figure 5 also illustrates the peak positions from the (531) and ($\bar{5}\bar{3}\bar{1}$) surfaces that were predicted by CrystalMaker software using the diffraction conditions used in the experiment. In the simulation, a virtual fcc Cu crystal was oriented to expose the (531) plane, and rotations through ψ and ϕ were performed to simulate the experimental diffraction geometry and identify the angular locations of the peaks from the (111), (200), (220), and (331) planes. The simulation was then repeated for the ($\bar{5}\bar{3}\bar{1}$) surface.

In the experimental scans, absolute azimuthal angles are arbitrary and only relative positions are useful. In the diffraction pattern from the (531)-oriented crystal (Figure 5), the peak from the (200) plane is located at an angle ~133° *less* than the peak from the (111) plane. In the diffraction pattern from the ($\bar{5}\bar{3}\bar{1}$)-oriented crystal, the peak from the ($\bar{2}00$) plane is located at an angle ~133° *greater* than the peak from the ($\bar{1}\bar{1}\bar{1}$) plane. The direction of rotation about the surface normal of the crystal face remains constant for each experiment; thus, a clockwise rotation for one surface corresponds to a counterclockwise rotation for its enantiomorph. It is clear from the experimental and from the predicted diffraction patterns that a clockwise rotation of the diffraction pattern for the (531) surface is equivalent to a counterclockwise rotation of the ($\bar{5}\bar{3}\bar{1}$) surface. The predicted spacing of the peaks for the two surfaces can then be aligned with those observed experimentally to identify the absolute

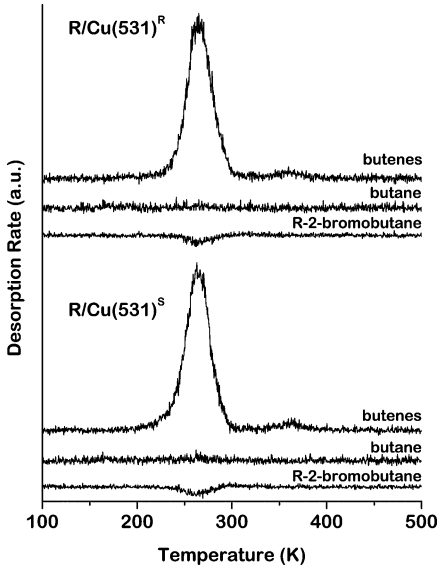

Figure 6. TPR spectra of a low coverage of *R*-2-bromobutane on Cu(643)$^{R\&S}$. Butene is the only product, and it evolves at the same temperature on both enantiomeric faces of Cu(643); therefore, the enantioselectivity toward debromination and β-hydride elimination are $ES_{\beta H} = ES_{Br} = 1$.

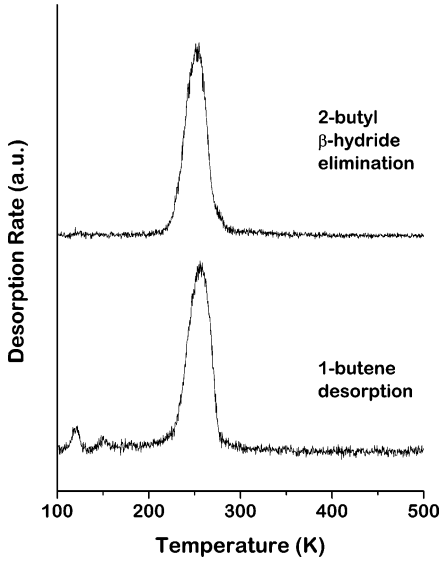

Figure 7. Comparison between the TPR spectra of butene produced by β-hydride elimination in *R*-2-butyl groups and the desorption of *trans*-2-butene after direct molecular adsorption on the Cu(643)^R surface. A low coverage was used in both cases to probe only the effects of reaction and desorption at the kink sites. The peak temperature of *trans*-2-butene desorption is similar to the peak temperature of butene production from β-hydride elimination; therefore, the evolution of butene from β-hydride elimination is desorption rate limited.

orientations of the (531) and ($\bar{5}\bar{3}\bar{1}$) surfaces and thus assign their chirality as (531)^R or (531)^S.

3.2. Low-Coverage Surface Chemistry of *R*-2-Bromobutane on Cu(643)$^{R\&S}$. *R*-2-Bromobutane, CH_3*$CH(Br)CH_2CH_3$, was chosen as the probe of enantioselective reactivity on the chiral Cu(643) and Cu(531) surfaces because it is the simplest, chiral alkyl bromide. The chemical structure of *R*-2-bromobutane is shown at the top of Figure 2. The substituents around the chiral carbon atom are a bromine atom, an ethyl group, a methyl group, and a hydrogen atom. Assuming that there is no racemization during debromination, the intermediate 2-butyl group is the simplest chiral alkyl group that can be tethered to a surface through its chiral carbon atom.

The chemistry of *R*-2-bromobutane on Cu surfaces generates three gas-phase products during heating: *R*-2-bromobutane by molecular desorption, butenes from β-hydride elimination of *R*-2-butyl groups, and butane from hydrogenation of the *R*-2-butyl groups. The yield of *R*-2-bromobutane with respect to the total product yield serves as a measure of the selectivity toward desorption, while the sum of the yields of butane and butene serves as a measure of the selectivity toward debromination. The yields of butene and butane serve as measures of the selectivities toward the β-hydride reaction and the hydrogenation reaction, respectively (see Appendix A).

A low initial coverage of ~0.15 monolayers was used to study the surface chemistry of *R*-2-bromobutane on the chiral kink sites with minimal influence from achiral step and terrace sites. This low coverage was produced by exposing the surface to 1 L of *R*-2-bromobutane under conditions at which an exposure of 7 L saturated the monolayer. Desorption spectra of butene, the β-hydride elimination product, from the Cu(643)^R and Cu(643)^S surfaces are shown in Figure 6. The peak desorption temperature was $T_p = 254$ K and ~100% of the *R*-2-bromobutane was converted into butene. The TPR spectra from the two surfaces show no significant difference in either the peak desorption temperatures or the product yields. Furthermore, the TPR spectra of racemic 2-bromobutane from the Cu(643)^R and Cu(643)^S surfaces are identical to those of *R*-2-bromobutane. Therefore, the selectivity to debromination was $S = 1$ and the selectivity of β-hydride elimination was $S = 1$ on both surfaces, resulting in enantioselectivities of $ES = 1$.

To probe the reaction kinetics for butene production, the temperature-programmed desorption spectrum of *trans*-2-butene on the Cu(643)^R surface was compared to the butene desorption spectrum obtained during TPRS of *R*-2-bromobutane at low coverage. The peak desorption temperatures, as illustrated in Figure 7, are almost identical. This implies that the kinetics of butene desorption during TPRS of *R*-2-bromobutane are limited by its desorption rate constant, k_6, rather than the rate constant for β-hydride elimination, k_3; thus, it is not surprising that the butene peak desorption temperature does not exhibit any enantiospecificity. It is also the case that, because the surface chemistry of *R*-2-bromobutane yields only one product at low coverage, the product yield cannot be enantioselective.

3.3. Monolayer Coverage Surface Chemistry of *R*-2-Bromobutane on Cu(643)$^{R\&S}$. The TPR spectra obtained for monolayer coverages of *R*-2-bromobutane on the Cu(643)^R and Cu(643)^S surfaces (Figure 8) are considerably different from the low-coverage spectra (Figure 6). At monolayer coverage, all reactive sites are populated with *R*-2-bromobutane. There is evidence of both *R*-2-bromobutane desorption and debromination to form 2-butyl groups. In addition to β-hydride elimination of the 2-butyl groups to yield butene, there is evidence of 2-butyl hydrogenation to butane. More importantly, there are subtle differences in the yields of the three products from the two different surfaces. The differences in the amounts of *R*-2-bromobutane, butene, and butane desorbing from the Cu(643)^R and Cu(643)^S surfaces are small yet reproducible. There is slightly more butene produced on the Cu(643)^R surface than on the Cu(643)^S surface, and slightly more butane produced on the Cu(643)^S surface than on the Cu(643)^R surface. Although the total yield of 2-bromobutane from either surface is small, there is almost twice as much *R*-2-bromobutane desorbing from the Cu(643)^S surface as from the Cu(643)^R surface. The most noticeable difference between the spectra obtained from the two surfaces is the appearance of the high-temperature desorption

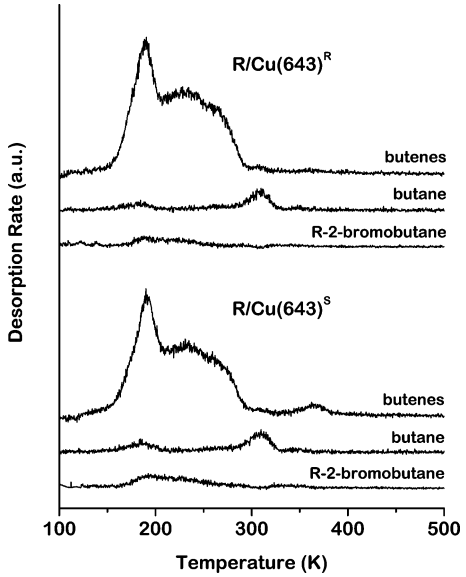

Figure 8. TPD spectra of monolayer coverage of *R*-2-bromobutane on $Cu(643)^{R\&S}$. *R*-2-bromobutane desorbs and reacts to form different amounts of *R*-2-bromobutane and butane that depend on the chirality of the surface. The enantioselectivities are $ES \neq 1$.

TABLE 1: Enantioselectivities (*ES*) and Enantiomeric Excesses (*ee*) of Desorption, Debromination, *β*-hydride Elimination, and Hydrogenation for *R*-2-bromobutane on the $Cu(643)^{R\&S}$ and $Cu(531)^{R\&S}$ Surfaces

	$Cu(643)^{R\&S}$		$Cu(531)^{R\&S}$	
	ES	*ee* (%)	*ES*	*ee* (%)
R-2-bromobutane (desorption)	0.61 ± 0.10	24	0.36 ± 0.13	47
R-2-butyl (debromination)	1.04 ± 0.07	2.0	1.18 ± 0.09	8.3
butene (*β*-hydride elimination)	1.05 ± 0.06	2.4	1.20 ± 0.08	9.1
butane (hydrogenation)	0.80 ± 0.11	11	1.00 ± 0.06	0.0

of butene at 366 K from the $Cu(643)^S$ surface. On $Cu(643)^S$, 3% of the total butene yield desorbs at 366 K. There is no discernible butene desorption from the $Cu(643)^R$ surface at this temperature. The simple fact that this high-temperature peak does not appear in the butene desorption spectrum for $Cu(643)^R$ indicates that the decomposition process is enantioselective.

The *R*-2-bromobutane and butene desorption peaks are very broad and thus cannot be used to detect enantiospecific surface reaction kinetics. Moreover, following *β*-hydride elimination, the appearance of butene is desorption rate limited. Butene is achiral, and thus, the kinetics of butene desorption during the TPR experiment cannot be used to probe enantioselectivity, and we must rely on its yield with respect to the other products.

The last feature to note in the monolayer coverage TPR spectra from the $Cu(643)^{R\&S}$ surfaces is the apparent butane desorption peak that appears at 308 K. If this peak is due to butane desorption, it is likely that it arises from some additional reaction pathway such as butene hydrogenation rather than direct butyl hydrogenation. The enantioselectivities derived from the analysis of the TPR spectra are the same whether one includes this contribution or not.

Three sets of *R*-2-bromobutane TPR spectra were obtained on both the $Cu(643)^R$ and the $Cu(643)^S$ surfaces to assess the reproducibility of the product desorption yields. The yields of desorption and debromination during *R*-2-bromobutane reaction on the $Cu(643)^{R\&S}$ surfaces reveal enantioselectivities of $ES_{des} = 0.61 \pm 0.10$ and $ES_{Br} = 1.04 \pm 0.07$, respectively. The yields of *β*-hydride elimination and hydrogenation during *R*-2-butyl decomposition on the $Cu(643)^{R\&S}$ surfaces reveal enantioselectivities of $ES_{\beta H} = 1.05 \pm 0.06$ and $ES_H = 0.80 \pm 0.11$,

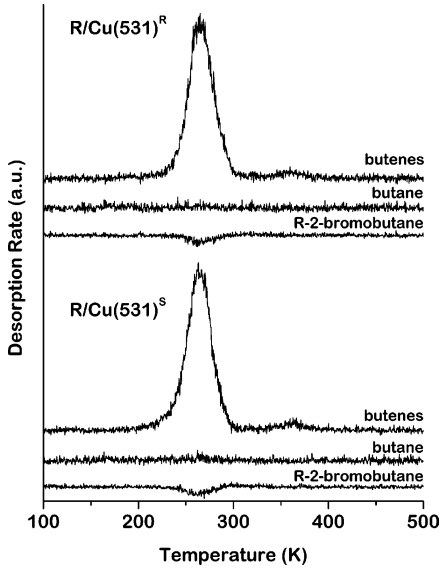

Figure 9. TPR spectra of a low coverage of *R*-2-bromobutane on $Cu(531)^{R\&S}$. Butene is the only product and it evolves at the same temperature on both enantiomeric faces of Cu(531); therefore, the enantioselectivity toward debromination and *β*-hydride elimination are $ES_{\beta H} = ES_{Br} = 1$.

respectively. Table 1 shows the enantioselectivities and enantiomeric excesses for desorption and debromination of *R*-2-bromobutane on Cu(643) and for *β*-hydride elimination and hydrogenation of *R*-2-butyl groups on Cu(643). The fact that ES_{des} and ES_H are significantly different from unity is clear evidence of enantioselective surface chemistry. As expected, the control experiments using rac-2-bromobutane yielded identical desorption yields from both the $Cu(643)^R$ and the $Cu(643)^S$ surfaces or, in other words, enantioselectivities of $ES = 1$, indicating no enantioselectivity.

3.4. Low Coverage of *R*-2-Bromobutane on $Cu(531)^{R\&S}$. To study the effects of surface structure on the enantioselectivity of *R*-2-bromobutane surface chemistry, the results of our measurements on the $Cu(643)^{R\&S}$ surfaces have been compared to the results of a similar set of measurements made on the $Cu(531)^{R\&S}$ surfaces. Initially, a low coverage of *R*-2-bromobutane was produced by exposing the $Cu(531)^{R\&S}$ surfaces to a 1 L exposure of *R*-2-bromobutane vapor. The TPR spectra for the low coverage of *R*-2-bromobutane on $Cu(531)^{R\&S}$ are shown in Figure 9. The only product desorbing from the surface is butene. The peak desorption temperature of butene was 265 K from both $Cu(531)^{R\&S}$ surfaces, and ~100% of the *R*-2-bromobutane converted to *R*-2-butyl and then to butene. This butene desorption temperature is roughly 10 K higher than that on the $Cu(643)^{R\&S}$ surfaces. The selectivity toward debromination of the 2-bromobutane was $S = 1$, and the selectivity toward *β*-hydride elimination in the *R*-2-butyl group was $S = 1$ on both surfaces. The TPR spectra of racemic 2-bromobutane and *R*-2-bromobutane on the $Cu(531)^{R\&S}$ surfaces are identical at low coverages. As on the $Cu(643)^{R\&S}$ surfaces, at a low coverage of *R*-2-bromobutane on $Cu(531)^{R\&S}$, the enantioselectivities are $ES = 1$ or, in other words, there is no enantioselectivity.

3.5. Monolayer Coverage of *R*-2-Bromobutane on $Cu(531)^{R\&S}$. The TPR spectra obtained from a monolayer coverage of *R*-2-bromobutane on the $Cu(531)^{R\&S}$ surfaces (Figure 10) are much different from those obtained at low coverage. The monolayer was produced by an exposure of 7 L to the vapor. During heating, desorption of *R*-2-bromobutane occurs in the temperature range 150−300 K, but it is accompanied by a

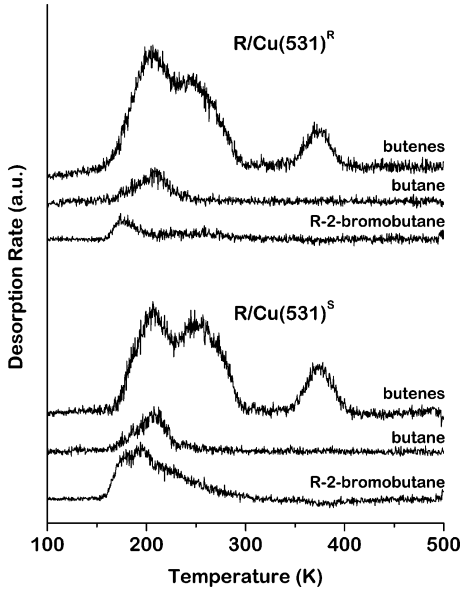

Figure 10. TPR spectra of monolayer coverage of *R*-2-bromobutane on Cu(531)$^{R\&S}$. *R*-2-bromobutane desorbs and reacts to form different amounts of *R*-2-bromobutane, *R*-2-butyl, and butene that depend on the chirality of the surface. The enantioselectivities are $ES \neq 1$.

significant amount of debromination to yield *R*-2-butyl groups. These *R*-2-butyl groups undergo β-hydride elimination to yield butene, which then desorbs in the temperature range 150−300 K and in a high-temperature desorption feature at 375 K. Although the Cu(531)$^{R\&S}$ surfaces do not have well-defined terrace-step-kink structures, it appears that there are multiple sites from which butene desorption occurs because there are multiple peaks in the desorption spectra. In addition to β-hydride elimination to yield butene, there is evidence of hydrogenation of 2-butyl groups to produce butane. Comparison of the areas under each desorption curve in Figure 10 reveals approximately 3 times more *R*-2-bromobutane desorbing from Cu(531)^{S} than from Cu(531)^{R}. Thus there are fewer *R*-2-butyl groups produced on the Cu(531)^{S} surface than on the Cu(531)^{R} surface. In the low-temperature range, there is less butene produced on Cu(531)^{S} than on Cu(531)^{R}, but there are identical amounts of butene desorbing from both faces of Cu(531) in the peak at 375 K. Butane is produced in identical quantities on both the Cu(531)^{R} surface and the Cu(531)^{S} surface. Although it would seem that butane production is not indicative of enantioselectivity, the fact that there are fewer *R*-2-butyl groups on the Cu(531)^{S} surface than on the Cu(531)^{R} surface means that, of the *R*-2-butyl groups remaining on each surface, a higher fraction are hydrogenated on Cu(531)^{S} than on Cu(531)^{R}. The control experiments using racemic 2-bromobutane resulted in identical desorption yields from both the Cu(531)^{R} and the Cu(531)^{S} surfaces. Thus, R-2-bromobutane desorption, butene production, and butane production from *R*-2-bromobutane are all indicative of enantioselective surface chemistry on the Cu(531)$^{R\&S}$ surfaces.

There are three distinct peaks in the butene spectra from the Cu(531)$^{R\&S}$ surfaces. The first peak appears at 210 K, the second at 250 K, and the third at 375 K. On Cu(531), ~14% of the total amount of butene produced desorbs at 375 K. Although the *R*-2-bromobutane desorption peaks appear at slightly different temperatures on the Cu(531)$^{R\&S}$ surfaces, they are very broad, and desorption is competing with debromination in this temperature range; therefore, it is not possible to determine the origin of the apparent enantioselective difference in the *R*-2-bromobutane desorption temperatures from the two surfaces. As with the results on the Cu(643)$^{R\&S}$ surfaces, the selectivities of the reaction yields on the Cu(531)$^{R\&S}$ surfaces will be used as the basis for quantification of enantioselectivities.

Three sets of *R*-2-bromobutane TPD spectra were obtained on both the Cu(531)^{R} and the Cu(531)^{S} surfaces to assess the reproducibility of the desorption yields. The yields of desorption and debromination during *R*-2-bromobutane reaction on the Cu(531)$^{R\&S}$ surfaces reveal enantioselectivities of $ES_{des} = 0.36 \pm 0.13$ and $ES_{Br} = 1.18 \pm 0.09$, respectively. The yields of β-hydride elimination and hydrogenation during *R*-2-butyl decomposition on the Cu(531)$^{R\&S}$ surfaces reveal enantioselectivities of $ES_{\beta H} = 1.20 \pm 0.08$ and $ES_{H} = 1.00 \pm 0.06$, respectively. Table 1 shows the enantioselectivities and enantiomeric excesses for all of the reactions toward their respective products for *R*-2-bromobutane on the Cu(531)$^{R\&S}$ surfaces. The control experiments using racemic 2-bromobutane produced identical desorption yields from both the Cu(531)^{R} and the Cu(531)^{S} surfaces, indicating no enantioselectivity for reactions of racemic 2-bromobutane.

4. Discussion

The mechanism of *R*-2-bromobutane decomposition on Cu surfaces is complex and is illustrated in Figure 2. There are six possible elementary reaction steps with rate constants for each reaction denoted as k_i. The mechanism of *R*-2-bromobutane decomposition on Cu surfaces is, in reality, more complex than illustrated by the simple model in Figure 1. There are three possible products of β-hydride elimination in the *R*-2-butyl group: 1-butene, *cis*-2-butene, and *trans*-2-butene. Previous work has shown that β-hydride elimination is favored at secondary carbon atoms over primary carbon atoms, so the most likely products of β-hydride elimination in the *R*-2-butyl groups are *cis*-2-butene and *trans*-2-butene.[23] It is not possible, however, to discriminate between the three butenes on the basis of their fragmentation patterns; therefore, their rates of production have been represented by the combined rate constant, k_3. It is also important to point out that the terrace-step-kink structure of the Cu(643) and Cu(531) surfaces results in a high degree of surface heterogeneity, and the rate constants for each elementary must depend on the reaction site. Finally, butene production is rate limited by desorption rather than by β-hydride elimination; therefore, the rate of butene desorption is not indicative of the rate of β-hydride elimination. The overall mechanism is sufficiently complicated that it is not possible to derive elementary rate constants from the desorption spectra.

As a consequence of the complications mentioned above, reaction enantioselectivities were chosen as the measure of enantiospecific behavior. Although it is not possible to determine the absolute selectivities of the reaction steps leading to *R*-2-bromobutane, butene, and butane desorption, it is possible to determine the enantioselectivity, ES_x, to product x (see Appendix A). The enantioselectivity is defined as the ratio of the yield, Y_x^R, of product x from the *R*- surface to the yield of product x from the *S*- surface.

$$ES_x = \frac{Y_x^R}{Y_x^S}$$

These have then been used to define the enantioselectivities of the reactions that are responsible for producing each product: desorption (ES_{des}), debromination (ES_{Br}), β-hydride elimination ($ES_{\beta H}$), and hydrogenation (ES_H).

4.1. Low Coverage of *R*-2-Bromobutane on Cu(643)$^{R\&S}$ and Cu(531)$^{R\&S}$. On both the Cu(643)$^{R\&S}$ and Cu(531)$^{R\&S}$ surfaces, the selectivity toward desorption of the *R*-2-bromo-

butane at low coverage was $S_{des} = 0\%$, and the selectivity toward β-hydride elimination in the *R*-2-butyl groups was $S_{\beta H} = 100\%$. This was observed on both the *R*- and *S*- enantiomers of the surfaces; therefore, no enantioselectivity was detected. It is important to note that this result does not mean that there is a lack of enantiospecificity to the rate constants for debromination, k_2^R and k_2^S, on the two chiral surfaces. It simply means that the rate constants for debromination, k_2^R and k_2^S, are significantly greater than the desorption rate constants k_1^R and k_1^S; thus, there is no observable molecular desorption of *R*-2-bromobutane.

The yields of butene and butane from the reactions of the *R*-2-butyl groups could reveal enantioselectivity; however, the complete lack of butane desorption at low coverages means that the selectivity for butene production was $S = 100\%$ on both the *R*- and *S*- faces of the Cu(643) and Cu(531) crystals. In this case, the rate constants for β-hydride elimination, k_3^R and k_3^S, are both significantly higher than those for hydrogenation, k_4^R and k_4^S; thus, there is no production of butane and no opportunity to observe enantioselective butane production.

In principle, the rate constants for β-hydride elimination, k_3^R and k_3^S, must be enantiospecific, and the kinetics of β-hydride elimination should be different on the two enantiomers of the Cu(643) and Cu(531) surfaces. At low coverages of *R*-2-bromobutane, however, the peak desorption temperatures for butene are the same regardless of the chirality of the two surfaces. Enantiospecific desorption kinetics are not observable because the kinetics of butene evolution from the surface are rate limited by desorption rather than by β-hydride elimination. TPR spectra of *trans*-2-butene desorption were obtained on Cu(643) and Cu(531), and the desorption peak temperatures of *trans*-2-butene were within 5 K of the desorption peak temperatures of butene produced by β-hydride elimination (Figure 7). The results of previous work suggest that the peak temperature for β-hydride elimination of *R*-2-bromobutyl groups is probably less than 215 K. This is the peak desorption temperature observed for the desorption of ethylene from the Cu(221) surface during the temperature-programmed reaction of ethyl iodide.[24] In that case, the peak ethylene desorption temperature is rate limited by β-hydride elimination rather than desorption. The greater chain length of the butene increases its heat of adsorption, causing it to desorb at a higher temperature than ethylene. Although the kinetics of β-hydride elimination should be enantiospecific on the $Cu(643)^{R\&S}$ and $Cu(531)^{R\&S}$ surfaces, the butene products are not chiral, and therefore, their desorption kinetics cannot be enantiospecific.

4.2. Monolayer Coverage of *R*-2-Bromobutane on $Cu(643)^{R\&S}$ and $Cu(531)^{R\&S}$. Enantioselective surface chemistry was observed at monolayer coverages of *R*-2-bromobutane on the Cu(643) and Cu(531) surfaces, and the enantioselectivities and enantiomeric excesses of each reaction are listed in Table 1. On Cu(643), desorption displayed an $ES_{des} = 0.61$, and on Cu(531), desorption displayed an $ES_{des} = 0.36$. On Cu(531), debromination displayed an $ES_{Br} = 1.18$. On Cu(643), hydrogenation displayed an $ES_H = 0.80$, and on Cu(531), β-hydride elimination displayed an $ES_{\beta H} = 1.20$. These results indicate that, at monolayer coverage, molecular *R*-2-bromobutane and *R*-2-butyl groups sense their chiral environments on these surfaces. This is almost certainly true at lower coverages but is undetectable because the relative magnitudes of the rates constants lead to 100% butene production. Unfortunately, even at the high coverages at which enantioselectivity is observed, it is not possible to determine which elementary reactions lead to the enantioselectivity.

The enantioselectivities and enantiomeric excesses of desorption and debromination are greater on Cu(531) than on Cu(643), and greater than the enantioselectivities and enantiomeric excesses of the reactions of the *R*-2-butyl groups. On the basis of this result, it appears that the surface chemistry of *R*-2-bromobutane is more enantioselective than that of *R*-2-butyl. It also appears that the different kink structures and kink densities of the Cu(643) and Cu(531) surfaces influence the enantioselectivities of desorption and debromination.

The interaction between a chiral molecule and a chiral substrate is complicated, and it is unlikely that any single measure of chirality will correlate with enantioselectivities in general. A recent study by Downs and Hazen seeks to quantify the "degree of chirality" of a variety of surfaces.[25] They define a chirality index based on the displacements of atoms from pseudomirror planes. In that study, the fcc(531) plane is found to be less chiral than the fcc(643) plane; therefore, it was expected that a Cu(643) surface would exhibit a larger enantiospecific effect than the Cu(531) surface. This is, of course, opposite to the observations reported in this work. Unfortunately, when assessing a surface's ability to catalytically differentiate between chiral molecules, the molecular structure and subsequent reactions impact the enantioselectivity as much as the "degree of chirality" of the surface.

In conjunction with a "degree of chirality" for surfaces, a "degree of chirality" should be considered for the molecular adsorbates and the specific elementary steps by which they react. As an example, *R*-2-butyl does not possess a significant asymmetry around the β-carbon atoms at which β-hydride elimination occurs. In fact, locally, the two reaction centers for β-hydride elimination are achiral, so any enantiospecificity is the result of nonlocal asymmetry. However, in *R*-2-bromobutane, the debromination center is the chiral center; therefore, a larger enantiospecific response might be expected during debromination. This is in fact what has been observed in the results reported here.

4.3. High-Temperature Butene Production. At monolayer coverages of *R*-2-bromobutane on both Cu(643) and Cu(531), butene is produced at high temperatures during heating. Figure 11 compares the TPR spectra of butene produced at high temperature. On the basis of a previous study,[26] this effect is attributed to caging of alkyl groups on defect sites by bromine atoms. The exact caging mechanism is unknown, but it is thought that β-hydride elimination is prevented because the alkyl group requires an empty, adjacent site to which it can transfer the hydrogen atom. If no site is available for this two-site process (and there is no alternative reaction pathway), then β-hydride elimination cannot proceed until the temperature is high enough to promote bromine atom diffusion away from the alkyl group. Once the bromine cage is broken, the reaction can proceed rapidly. On Cu(643) butene is produced at 366 K, and on Cu(531), butene is produced at 375 K. This temperature difference indicates that the bromine atoms diffuse more rapidly on Cu(643) than on Cu(531). The small dimensions of the unit cell on Cu(531) might inhibit bromine atom diffusion to a greater extent than the open geometry of Cu(643). The yield of high-temperature butene on the $Cu(643)^{R\&S}$ surfaces is also enantiospecific; far more butene desorbs at high temperature from the $Cu(643)^S$ surface than from the $Cu(643)^R$ surface. This suggests that the kinetics of β-hydride elimination are faster on the $Cu(643)^R$ surface than on the $Cu(643)^S$ surface and, thus, that there are fewer 2-butyl groups left on the $Cu(643)^R$ surface to be trapped by adsorbed Br atoms.

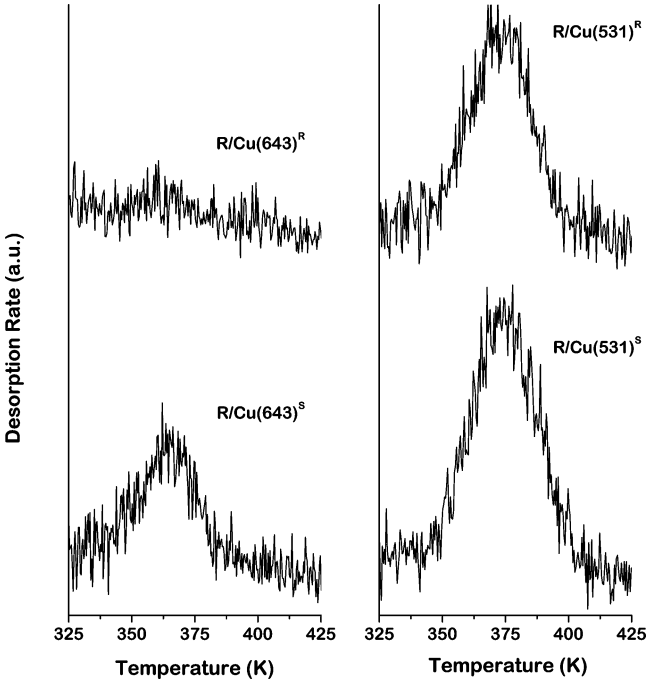

Figure 11. A comparison of the high-temperature butene desorption from Cu(643)$^{R\&S}$ and Cu(531)$^{R\&S}$. Butene production exhibits enantioselectivity on the Cu(643) surfaces but not on the Cu(531) surfaces.

5. Conclusions

Enantioselectivity has been observed in the surface chemistry of *R*-2-bromobutane and *R*-2-butyl groups on the Cu(643)$^{R\&S}$ surfaces and on the Cu(531)$^{R\&S}$ surfaces. The enantioselectivities of desorption and debromination indicate a higher degree of enantioselectivity on the Cu(531)$^{R\&S}$ surfaces than on the Cu(643)$^{R\&S}$ surfaces, while the enantioselectivities of β-hydride elimination and hydrogenation indicate a similar degree of enantioselectivity on both surfaces. In addition, it has been demonstrated that, under conditions such as low coverage where the net selectivity of a reaction to butene is 100%, it is impossible to observe any enantiospecificity of the underlying rate constants. This will be generally true of all such surface reactions and limit the applicability of selectivity as a means of probing enantiospecific surface reaction rate constants. Clearly, the surface structure impacts the enantioselectivity, but it is unclear whether these effects are due to kink density or kink structure. The relative contributions of kink structure and kink density to the enantioselectivities of surface reactions can only be explored by an extensive study of surfaces with different kink structures and with varying kink densities.

Acknowledgment. This research was supported through the MRSEC program of the NSF under the award number DMR-0079996. K.S.K. would like to thank the donors of the American Chemical Society Petroleum Research Fund for partial support of his research.

Appendix A. Calculations of Enantioselectivity for *R*-2-bromobutane Decomposition

Analysis of the TPR spectra of *R*-2-bromobutane decomposition on the Cu(643)$^{R\&S}$ and the Cu(531)$^{R\&S}$ surfaces to yield physically meaningful measures of enantioselectivity is somewhat complicated. The TPR spectra for *R*-2-bromobutane desorption and decomposition reveal the desorption of three species over a wide temperature range with complex reaction kinetics. These spectra cannot be interpreted in any simple model to yield desorption or reaction rate constants associated with the elementary steps of the mechanism described in the Discussion. Rather than relying on the desorption rates at given temperatures as probes of enantioselectivity, the integrated yields of the products were chosen as measures of selectivity. If reaction kinetics are enantiospecific, the relative yields of the products will depend on the chirality of the surface.

Product yields of the four reactions (desorption, debromination, β-hydride elimination, and hydrogenation) were used. During heating, the signals at *m/q* ratios of 56, 57, and 58 were monitored. The three reaction products (*R*-2-bromobutane, butene, and butane) each have different fragmentation patterns and different contributions to the signals at *m/q* ratios of 56, 57, and 58. The three equations that relate the measured signal intensities at each *m/q* ratio, I_m, to the partial pressures of the desorbing products, P_x, are:

$$I_{56} = \alpha_{56,\text{butene}}P_{\text{butene}} + \alpha_{56,\text{butane}}P_{\text{butane}} + \alpha_{56,\text{bromobutane}}P_{\text{bromobutane}}$$

$$I_{57} = \alpha_{57,\text{butene}}P_{\text{butene}} + \alpha_{57,\text{butane}}P_{\text{butane}} + \alpha_{57,\text{bromobutane}}P_{\text{bromobutane}}$$

$$I_{58} = \alpha_{58,\text{butene}}P_{\text{butene}} + \alpha_{58,\text{butane}}P_{\text{butane}} + \alpha_{58,\text{bromobutane}}P_{\text{bromobutane}}$$

The coefficients, $\alpha_{m,x}$, are the sensitivities of the signals at a given mass, *m*, to the partial pressure of product *x*. Given the matrix of sensitivities, the partial pressures of each desorbing product can be calculated as a function of surface temperature from the TPR spectra. In a TPR spectrum, the partial pressure of the desorbing species at a given temperature is proportional to its rate of desorption, so the integrated partial pressure over the temperature range of the spectrum is proportional to the product yield, Y_x. Using a constant heating rate, β, results in the following expression for the product yield.

$$Y_x \propto \int_{T_0}^{T_{\max}} P_x \, \mathrm{d}T$$

The sensitivities, $\alpha_{m,x}$, were determined by introducing the pure compounds *R*-2-bromobutane, butene, and butane into the chamber and measuring the signals at *m/q* = 56, 57, and 58 for each over a range of pressures. The pressures of the three compounds were measured using an ion gauge, which, unfortunately, has different sensitivities for the three. The real partial pressure of a given compound, P_x, is related to the pressure measured by the ion gauge, P_x^{ig}, by a sensitivity factor, γ_x.

$$P_x = \gamma_x P_x^{\text{ig}}$$

Although the sensitivities of the ion gauge for butene and butane are likely to be similar to one another, they are not likely to be similar to the ion gauge sensitivity for *R*-2-bromobutane. Using the values of $\alpha_{m,x}$ to decompose the TPR signals into the partial pressures of each product actually yields values of P_x^{ig} at each temperature rather than values of the true partial pressure, P_x. Integration of these values of P_x^{ig} gives a product yield, Y_x^{ig}, that is related to the real product yield by

$$Y_x = \gamma_x Y_x^{\text{ig}}$$

The selectivities of the *R*-2-bromobutane decomposition reaction to the three different products are given by

$$S_x = \frac{Y_x}{Y_{\text{bromobutane}} + Y_{\text{butane}} + Y_{\text{butene}}} = \frac{\gamma_x Y_x^{\text{ig}}}{\gamma_{\text{bromobutane}} Y_{\text{bromobutane}}^{\text{ig}} + \gamma_{\text{butane}} Y_{\text{butane}}^{\text{ig}} + \gamma_{\text{butene}} Y_{\text{butene}}^{\text{ig}}}$$

The yields of products are dependent on the chirality of the Cu surface, so the selectivity of the *R*-enantiomer of 2-bromobutane on the Cu(*hkl*)$^{\text{R}}$ surface is expressed in the following equation:

$$S_x^{\text{R/R}} = \frac{Y_x^{\text{R/R}}}{Y_{\text{bromobutane}}^{\text{R/R}} + Y_{\text{butane}}^{\text{R/R}} + Y_{\text{butene}}^{\text{R/R}}}$$

The three reactions leading to the three products all have stoichiometries of one-to-one, so the total yield of products is simply equal to the initial coverage of *R*-2-bromobutane. We assume that the initial coverages of *R*-2-bromobutane are identical on both the *R*- and the *S*- surfaces, and thus that

$$Y_{\text{bromobutane}}^{\text{R/R}} + Y_{\text{butane}}^{\text{R/R}} + Y_{\text{butene}}^{\text{R/R}} = Y_{\text{bromobutane}}^{\text{R/S}} + Y_{\text{butane}}^{\text{R/S}} + Y_{\text{butene}}^{\text{R/S}}$$

Although the heats of adsorption on the two surfaces are different and the sticking coefficients on the two surfaces could be different, this assumption is born out by several observations. Following low exposures to *R*-2-bromobutane, the yields of butene from the *R*- and the *S*- surfaces are almost identical (Figures 6 and 9). Furthermore, in our prior studies of *R*-3-methylcyclohexanone adsorption on these surfaces, we have found that the coverages of the saturated monolayer on both surfaces are identical.[10,12] Finally, the enantioselectivity of the overall reaction toward a given product is

$$ES_x = \frac{S_x^{\text{R/R}}}{S_x^{\text{R/S}}} = \frac{Y_x^{\text{R/R}}}{Y_x^{\text{R/S}}} = \frac{(Y_x^{\text{ig}})^{\text{R/R}}}{(Y_x^{\text{ig}})^{\text{R/S}}}$$

These quantities can be measured directly from the areas of the TPR spectra measured for the three different products desorbing from the two enantiomers of a given surface. A value of $ES_x = 1$ indicates that no enantioselectivity is detected. The enantiomeric excess can also be calculated from measurable quantities, as shown in the following equation:

$$ee_x = \left|\frac{Y_x^{\text{R/R}} - Y_x^{\text{R/S}}}{Y_x^{\text{R/R}} + Y_x^{\text{R/S}}}\right| = \left|\frac{(Y_x^{\text{ig}})^{\text{R/R}} - (Y_x^{\text{ig}})^{\text{R/S}}}{(Y_x^{\text{ig}})^{\text{R/R}} + (Y_x^{\text{ig}})^{\text{R/S}}}\right|$$

The relationship between the enantioselectivity and the enantiomeric excess is simply

$$ee_x = \left|\frac{ES_x - 1}{ES_x + 1}\right|$$

Finally, throughout this paper, we refer to four different enantioselectivities obtained in the manner described above from the yields of three products measured during temperature-programmed reaction of *R*-2-bromobutane on the Cu(643)$^{\text{R\&S}}$ and Cu(531)$^{\text{R\&S}}$ surfaces.

Desorption: $$ES_{\text{des}} = \frac{Y_{\text{bromobutane}}^{\text{R/R}}}{Y_{\text{bromobutane}}^{\text{R/S}}}$$

Debromination: $$ES_{\text{Br}} = \frac{Y_{2-\text{butyl}}^{\text{R/R}}}{Y_{2-\text{butyl}}^{\text{R/S}}} = \frac{Y_{\text{butene}}^{\text{R/R}} + Y_{\text{butane}}^{\text{R/R}}}{Y_{\text{butene}}^{\text{R/S}} + Y_{\text{butane}}^{\text{R/S}}}$$

β-Hydride elimination: $$ES_{\beta\text{H}} = \frac{Y_{\text{butene}}^{\text{R/R}}}{Y_{\text{butene}}^{\text{R/S}}}$$

Hydrogenation: $$ES_{\text{H}} = \frac{Y_{\text{butane}}^{\text{R/R}}}{Y_{\text{butane}}^{\text{R/S}}}$$

Note that the ability to estimate the ratio of yields used to define the enantioselectivity for debromination is only possible because the ion gauge sensitivities of butene and butane are likely to be quite similar, $\gamma_{\text{butene}} \approx \gamma_{\text{butane}}$. The sensitivity for ethane is ~15% greater than that of ethylene, and the sensitivity for propane is ~15% greater than that of propylene. Thus the sum of the measured yields of butene and butane will be roughly proportional to the total coverage of 2-butyl groups on the surface. The fact that the desorption yields of butene are significantly higher than those of butane means that the assumption that $\gamma_{\text{butene}} \approx \gamma_{\text{butane}}$ introduces little error into the estimate of ES_{Br}. As noted in Table 1, the enantioselectivities of debromination and β-hydride elimination are quite similar.

References and Notes

(1) Orito, Y.; Imai, S.; Niwa, S.; Nguyen Gia, H. *Yuki Gosei Kagaku Kyokaishi* **1979**, *37*, 173−174.
(2) Izumi, Y. *Adv. Catal.* **1983**, *32*, 215−271.
(3) Hazen, R. M.; Filley, T. R.; Goodfriend, G. A. *Proc. Natl. Acad. Sci. U.S.A.* **2001**, *98*, 5487−5490.
(4) Sato, I.; Kadowaki, K.; Soai, K. *Angew. Chem., Int. Ed.* **2000**, *39*, 1510−1512.
(5) Ahmadi, A.; Attard, G.; Feliu, J.; Rodes, A. *Langmuir* **1999**, *15*, 2420−2424.
(6) Attard, G. A.; Ahmadi, A.; Feliu, J.; Rodes, A.; Herrero, E.; Blais, S.; Jerkiewicz, G. *J. Phys. Chem. B* **1999**, *103*, 1381−1385.
(7) Sholl, D. S.; Asthagiri, A.; Power, T. D. *J. Phys. Chem. B* **2001**, *105*, 4771−4782.
(8) McFadden, C. F.; Cremer, P. S.; Gellman, A. J. *Langmuir* **1996**, *12*, 2483−2487.
(9) Sholl, D. S. *Langmuir* **1998**, *14*, 862−867.
(10) Horvath, J. D.; Gellman, A. J. *J. Am. Chem. Soc.* **2002**, *124*, 2384−2392.
(11) Horvath, J. D.; Gellman, A. J. *J. Am. Chem. Soc.* **2001**, *123*, 7953−7954.
(12) Horvath, J. D.; Koritnik, A.; Kamakoti, P.; Sholl, D. S.; Gellman, A. J. *J. Am. Chem. Soc.* **2004**, *126*, 14988−14994.
(13) Attard, G. A. *J. Phys. Chem. B* **2001**, *105*, 3158−3167.
(14) Hazzazi, O. A.; Attard, G. A.; Wells, P. B. *J. Mol. Catal. A* **2004**, *216*, 247−255.
(15) Lin, J. L.; Bent, B. E. *J. Phys. Chem.* **1992**, *96*, 8529−8538.
(16) Lin, J.-L.; Teplyakov, A. V.; Bent, B. E. *J. Phys. Chem.* **1996**, *100*, 10721−10731.
(17) Forbes, J. G.; Gellman, A. J. *J. Am. Chem. Soc.* **1993**, *115*, 6277−6283.
(18) Zaera, F. *J. Phys. Chem.* **1990**, *94*, 8350−8355.
(19) Jenks, C. J.; Xi, M.; Yang, M. X.; Bent, B. E. *J. Phys. Chem.* **1994**, *98*, 2152−2157.
(20) Jenks, C. J.; Bent, B. E.; Zaera, F. *J. Phys. Chem. B* **2000**, *104*, 3017−3027.
(21) Goodwin, D. G.; Hudson, H. R. *J. Chem. Soc. B* **1968**, 1333−1336.
(22) Gellman, A. J.; Horvath, J. D.; Buelow, M. T. *J. Mol. Catal. A* **2001**, *167*, 3−11.
(23) Yang, M. X.; Teplyakov, A. V.; Bent, B. E. *J. Phys. Chem. B* **1998**, *102*, 2985−2990.
(24) Sung, D.; Gellman, A. J. *Surf. Sci.* **2004**, *551*, 59−68.
(25) Downs, R. T.; Hazen, R. M. *J. Mol. Catal. A* **2004**, *216*, 273−285.
(26) Jenks, C. J.; Paul, A.; Smoliar, L. A.; Bent, B. E. *J. Phys. Chem.* **1994**, *98*, 572−8.